Passive Microwave Radiometry in the Gobi-Desert Region

TENG XUYAN, SHI CHANGQING, and PENG HONGXIAN

Changchun Institute of Physics, Academia Sinica, Changchun, Jilin, China

XIAO JINKAI, LAI ZHAOSHENG, and YANG BOLIN

Guiyang Institute of Geochemistry, Academia Sinica, Guiyang, Guizhou, China

This paper summarizes preliminary results of remote sensing test with an airborne microwave radiometer, in the Gobi-desert region. The relationship between microwave signature and complex dielectric constant for various rocks and minerals is analyzed. The possibilities of exploring for water and mineral resources in this arid region by means of passive microwave radiometry are discussed.

Introduction

From September through November 1977, the Aerial Remote Sensing Program of Academia Sinica was carried out, in cooperation with the Department of Geology, for which, aerial geologic survey was the major goal. In China, this was the first comprehensive remote sensing test, and included a multispectral camera, an infrared scanner, a laser altimeter, and a microwave radiometer. The test field was located at the Paergang district, Hami, Xinjiang. The geographic coordinates are 41°25′ to 41°35′N and 90°21′ to 90°36′E, and the area is about 400 km^2. Paergang district is the vast and bare Gobi desert, with no sign of human habitation. The weather is extremely dry with mean annual rainfall of 32.7 mm. No permanent rivers are found here except intermittent streams which converge by surface runoff arising during the rainy season from July through August. Vegetation can hardly be found in most of the areas. The drought-enduring shrubs such as camel thorn grow only in some dry beds where the water regime is relatively well conditioned. So the rock series, on the whole, crop out on the surface completely. The major topography is denuded hills and accumulated plains with an average difference in height of about 150 m.

In order to investigate the microwave radiation properties of the rocks and minerals in the arid region, and probe the possibility of prospecting resources directly and indirectly with microwave radiometry, the test flights for experimental verification were performed. At the same time, a field survey and sampling were also conducted by geologic engineers. The dielectric property of samples taken from the test field was measured in the laboratory. The results of microwave radiometry demonstrated that the conclusions published earlier were further substantiated; e.g., any subsurface deposits probably have to be deduced indirectly from the knowledge of surface outcrops and faults by the aid of microwave radiometry (Bradford and Plaster, 1973).

Instrumentation and Data

The 3-cm airborne microwave radiometer developed by Changchun Institute of Physics, Academia Sinica, is shown in

52 Vanderbilt Ave., New York, NY 10017 0034-4257/84/$3.00

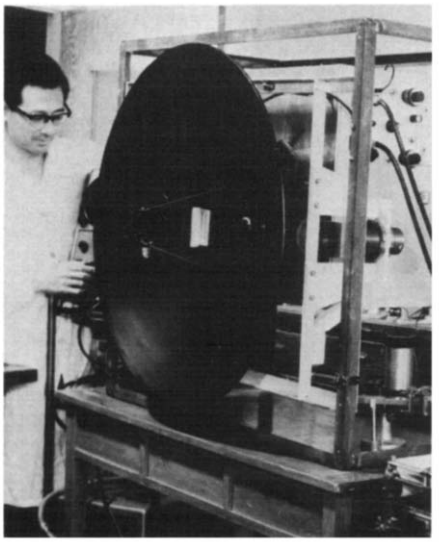

FIGURE 1. The airborne microwave radiometer.

Figure 1. It is a part of the null-balancing Dicke-type radiometer, with the response time being rapid enough and linearity being satisfactory due to a feedback servo loop (Zhang Junrong, 1980). A list of the microwave radiometer essential specifications is given in Table 1. Under the tests, the instruments were mounted on an E-14 aerial survey aircraft, the antenna window was closed by a radome (Figure 2).

On 26–28 October 1977, the microwave radiometer made flights over the test field four times, at an altitude of 3100 m. It was impossible to make a covering flight over the entire test field because of 150 m ground resolution; therefore, some sampling measurements were carried out. The microwave radiometric curves as output data were recorded on an *X-Y* recorder. Figure 3(a) gives six microwave radiometric curves acquired on 26 October 1977. The values of brightness temperature as shown in curves indicate the average radiation energy collected in six ground strips with 150 m width. The flight paths corresponding to these curves have been marked on the black-and-white infrared photograph of Paergang district, shown in Figure 3(b).

The Complex Dielectric Constant of Rocks and Minerals

The complex dielectric constant of a nonmagnetic, homogeneous, isotropic, semiinfinitely extended material having a smooth planar surface, as well as zero temperature gradient, completely characterizes the electromagnetic absorptivity of the material, under the condition of conservation of energy. As is well known, according to the relationship between the absorptivity (equal to the emissivity) and reflectivity, and utilizing the Fresnel formula, emissivity can be derived from the dielectric constant of rocks and minerals measured in the laboratory. This research method has been used universally so far.

Vickers and Rose (1971) have described in detail the method for measuring the complex dielectric constant of

TABLE 1 Specifications of the Microwave Radiometer

Center frequency	9200 MHz
Bandwidth IF	30 MHz
System's noise figure	$\leqslant 8$ dB
Brightness temperature sensitivity ($\tau = 1$ s)	1 K
Servo loop response time (2% allowable error)	32 ms
Dynamic range	100–300 K
Half-power beamwidth of the antenna	2°47′
Polarization mode	H

(a)

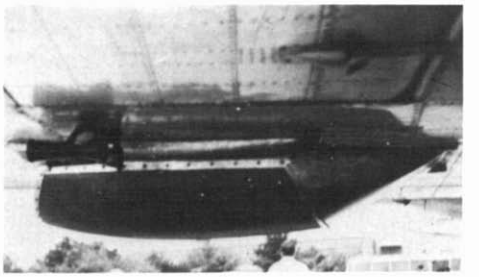

(b)

FIGURE 2. (a) E-14 aircraft utilized as a remote sensing platform and (b) radome.

rocks and minerals. The cavity perturbation method was adopted in our experiments for measuring complex dielectric constant, with a satisfactory accuracy for low loss material ($\tan\delta \leqslant 10^{-2}$). For stick samples, the calculation expressions are as follows:

$$\varepsilon' = 1 + \frac{1}{2} \cdot \frac{V_0}{V_s} \cdot \frac{f_0 - f_s}{f_0},$$

$$\varepsilon'' = \frac{1}{4} \cdot \frac{V_0}{V_s} \left(\frac{1}{Q_s} - \frac{1}{Q_0} \right),$$

where f_s and f_0 are the resonance frequencies of the cavity, with and without a rock sample, respectively, Q_s and Q_0 are the figures of merit of the cavity, with and without a rock sample, respectively, V_0 is the volume of the cavity, and V_s the volume of the rock sample. Table 2 gives the average complex dielectric constant (real part and imaginary part) of some typical samples at Paergang district, measured in the case of $f = 9286$ MHz. In addition, the average density and the theoretical computations for the average emissivity are also listed in Table 2.

These measurements were able to provide a sound basis for interpreting radiometric observations of similar materials in their natural environments and to develop a catalog of the microwave properties of rocks and minerals.

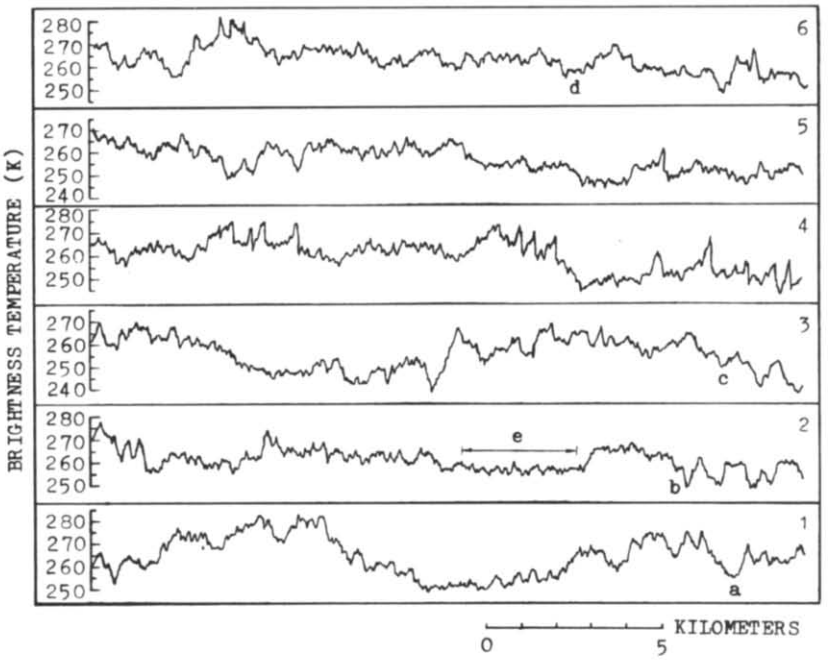

(a)

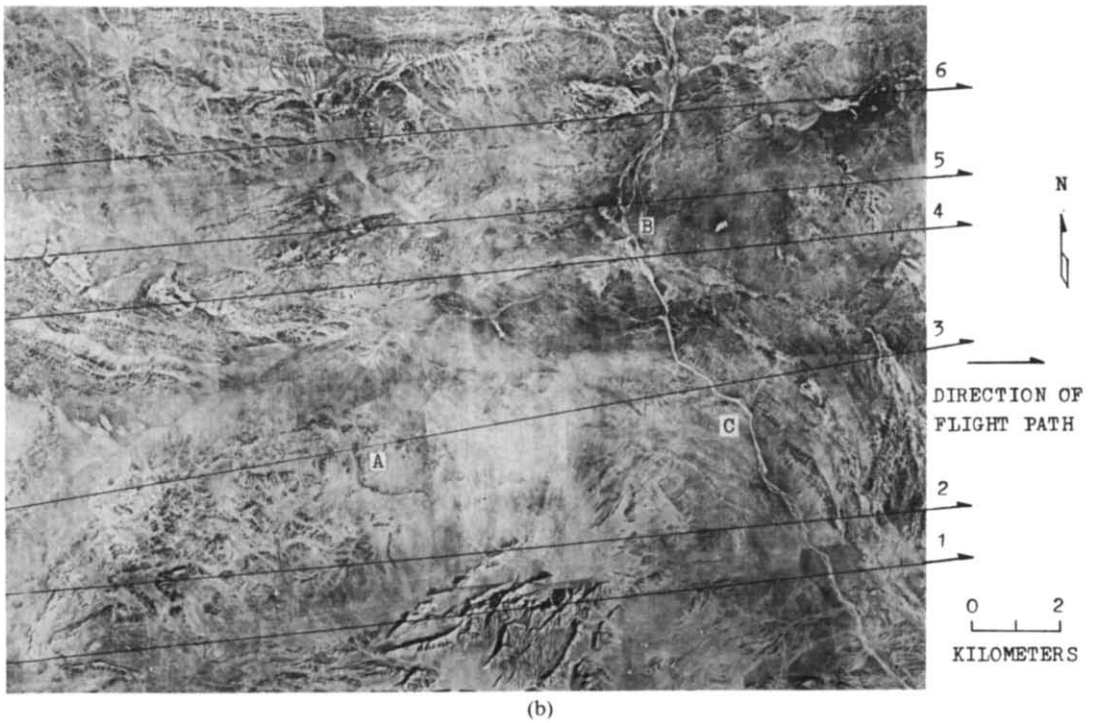

(b)

FIGURE 3. (a) Six microwave radiometric curves of Paergang district, acquired at an altitude of 3100 m on 26 October 1977 and (b) black and white infrared aerial mosaic of Paergang district in which the flight lines corresponding to these curves have been marked.

TABLE 2 The Complex Dielectric Constant (Real Part) ε', (Imaginary Part) ε'', Density, and Emissivity of Some Typical Rocks and Minerals of Paergang District

Name of Rocks and Minerals	Geologic Ages	Average ε'	Average ε''	Average Density	Average Emissivity
Sandstone	D_{1a}^{c}	4.14	0.033	2.64	0.884
Quartz-diorite	δ_4^{2-1A}	4.26	0.017	2.81	0.879
Slate	D_{1a}^{a}	4.34	0.174		0.875
Diorite porphyrite	$\delta'_{\mu A}$	4.50	0.027		0.871
Granite	γ_4^{2-3D}	4.61	0.046	2.67	0.867
Diorite	δ_4^{2-1A}	4.64	0.023	2.84	0.865
Tuffaceous sandstone	D_{1a}^{b}	4.95	0.077	2.64	0.856
Dolomite	P_{t_n}	6.18	0.019	2.83	0.818
Altered marble	D_{1a}^{b-3}	6.55	0.020	2.69	0.802
Marble	P_{t_n}	7.44	0.022		0.785
Limestone	P_{t_n}	7.73	0.023	2.61	0.778
Iron ore	P_{t_n}	22.23	1.680		

Earlier research work has indicated that the real part of the dielectric constant of rocks and minerals increases with increasing specific gravity (Edgerton and Trexler, 1970). Our research work shows, however, that not every kind of rock and mineral is in agreement with this conclusion. As shown in Table 2, the specific gravity among sandstone, granite, and limestone appears almost the same, but their dielectric constants prove to be different from each other. Based on our observation, it is essentially the porosity rather than the specific gravity that has a close association with the dielectric constant of rocks and minerals.

Analysis Results

As examples we show Figure 4, which includes the microwave radiometric curve, the curve of average dielectric constant, and geological factors sketch map of curves (flight lines) 1 and 3. In the center part of curve 1 [see Figure 4(a)], it is noted that a continual lower brightness temperature region, with an average value of about 250 K, corresponds to Quege Mountain system which is composed of dolomite-marble and marble of the Proterozoic Erathem. In the eastern part and the western part of curve 1, there are two high brightness temperature regions that correspond to, essentially, the interbedding of slate and tuffaceous sandstone, of the Devonian system. In addition, there are two valley points in the eastern part of curve 1, corresponding to a dry bed and a small area of deposit of the Quaternary Period, made up of clastic marble, respectively.

In Figure 4(b), a valley point in the center of curve 3 corresponds to the iron ore beds. Figure 5 is the multispectral color composite image of this area, i.e., the A area in Figure 3(b). These iron ore beds are depositional and metamorphic hematite-magnetite. It is an oskar emerging in an inverted S shape; the outlier area is not very large. Besides the iron ore beds, another relationship between the lithological character and the microwave radiometric curve is similar to that in Figure 4(a).

It can be seen from the above figures that various rocks and minerals exhibit different microwave signatures. It is clear that the higher the brightness temper-

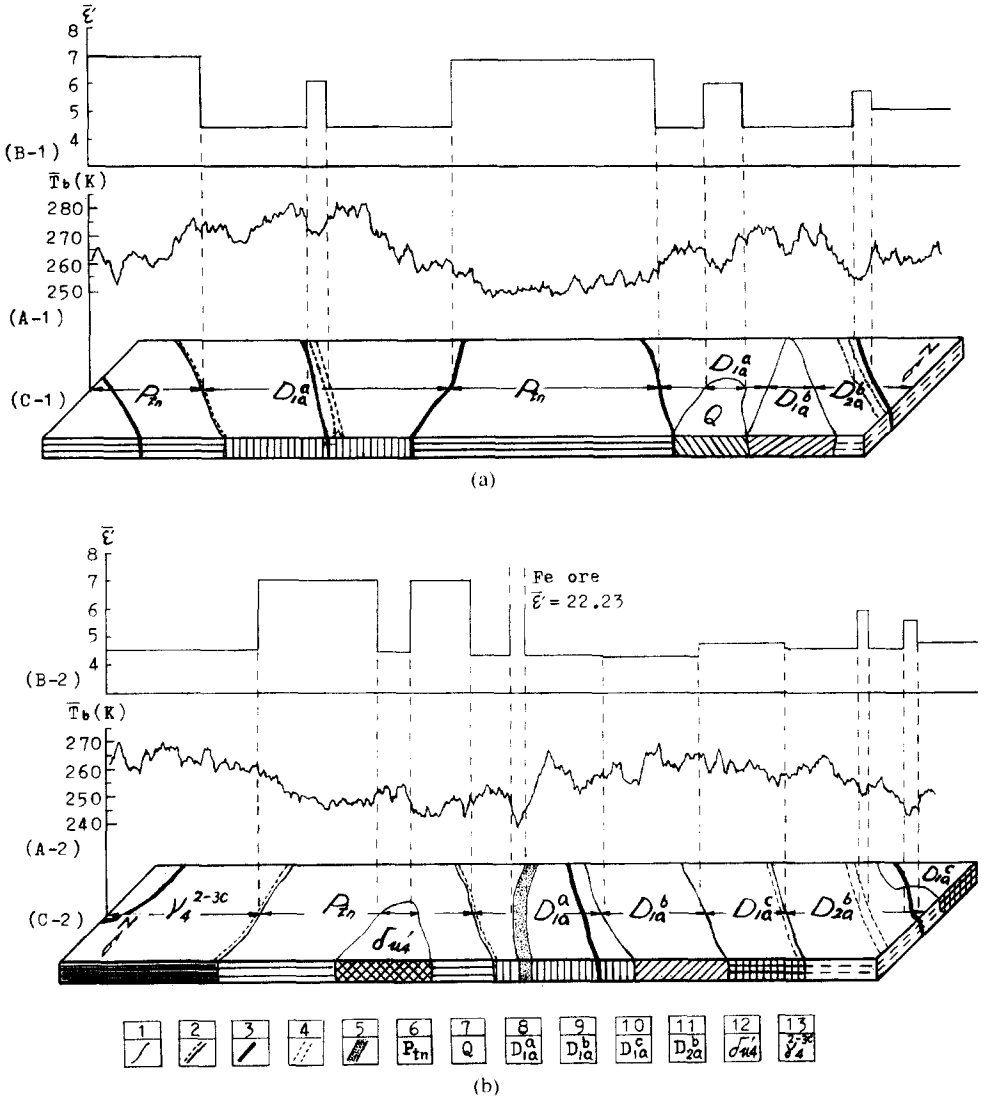

FIGURE 4. The contrast relation between microwave radiometric curve (A), average dielectric constant (B), and geological factors on the surface (C) for flight lines 1 (top) and 3 (bottom). Legend: (1) geological contact, (2) discordant boundary, (3) fault line, (4) dry bed, (5) the outcrop of iron ore, (6) dolomite-marble, marble, and limestone, (7) the deposit of the Quaternary Period, (8) sandstone, tuffaceous sandstone, and slate, (9) tuffaceous powdery sandstone and slate, (10) sandstone, slate mixed with limestone, (11) sandstone, at the bottom layer, interbedding of, sandstone, slate and marble at middle and top layer, (12) diorite porphyrite, and (13) granite.

ature, the lower the average complex dielectric constant. The relationship of growth and decline is the opposite. So, it is possible to distinguish various rocks and minerals due to different brightness temperature; for example, limestone, marble, and dolomite can be distinguished from sandstone, slate, and tuffaceous sandstone. Especially, as contrasted with surrounding rocks, the outcrop of iron ore appears in meaningful response.

It is noticed that the brightness temperature of the faults zone is lower than that on both sides of the faults. The

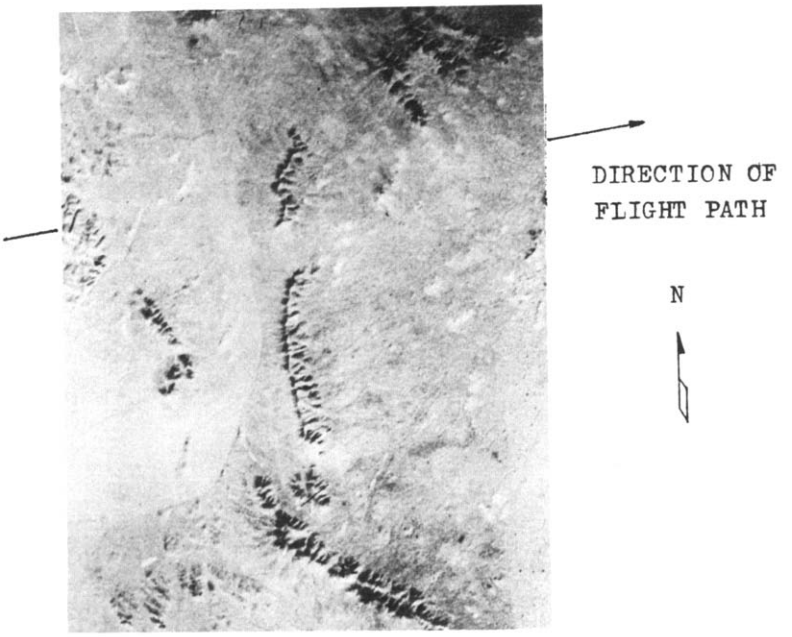

FIGURE 5. Multispectral composite image of the iron ore beds of the Paergang district.

tectonic geology tells us that some connections exist between faults and the water system. In Figure 3(b), the longest dry bed could be found. It is the major water system running through the test field from north to south and lies at some faults zone and tectonic lines, basically. In the B area, the longest dry bed is cut off by another large fault zone which runs from east to west; thus, the water system yields a significant change. Figure 6(a) is the multispectral color composite image of the B area; the outlines of the intersecting faults are clearly discernible. On the north of the faults zone, the water system is dispersed, while, on the south, it is converged afresh. From *in situ* observations we found the moisture-holding capacity on the north is a little better than that on the south, because the depositional layer over the water system on the north of the faults zone is composed of a porous and quite thick layer of sandy soil. For this reason, the coverage of shrubs on the north is also wider than that on the south.

When the fourth flight line and the fifth flight line passed through the southern and northern sides, respectively, the microwave radiometric curves presented similar lower value parts. Moreover, the average brightness temperature of curve 5 is somewhat lower than that of curve 4 [see Figure 6(b)]. There exists a difference of average brightness temperature between the northern side and the southern side, which is in close coincidence with the results of the surface observation. In addition, at all the intersecting points, at which flight lines cross over that the longest dry bed (e.g., a,b,c,d), and e section in curve 2 corresponding to a large faults zone called Xinger, there exist brightness temperature drops in varying degrees [see Figure 3(a)].

The dielectric constant (real part) ε' of rocks seems to vary somewhat at microwave frequencies, but a value of 5 is

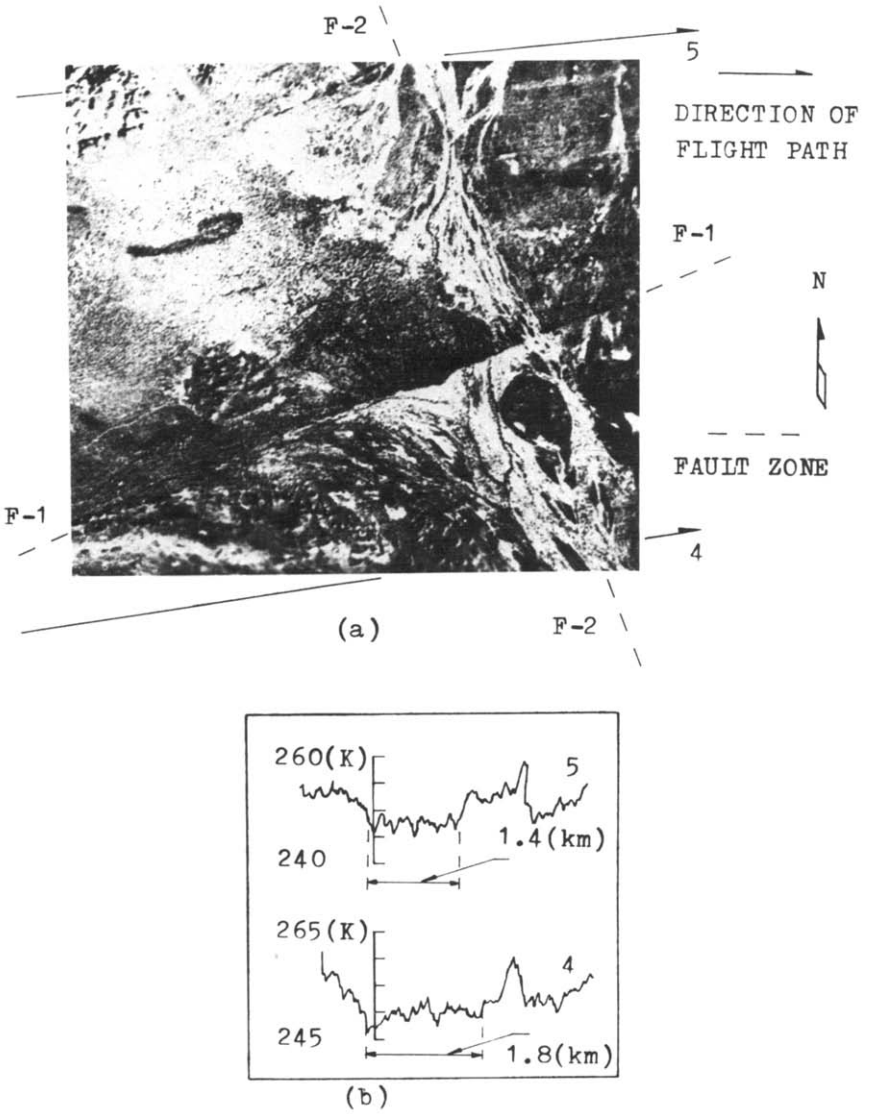

FIGURE 6. (a) Multispectral color composite image of intersecting faults at the eastern edge of the Paergang district and (b) microwave radiometric curves of this intersecting fault zone.

acceptable as an average for dry rocks, at a rough estimate; ε' for water, on the other hand, shows a remarkable drop at microwave frequencies from its value (78) at low frequencies. At a frequency of 10 GHz the value is about 50 according to Hoekstra and Cappilino (1971). The dielectric constant of water (real part), however, has been measured in our laboratory to be approximately 80 at low frequencies (at 20°C); and with 10 GHz, it is about 61 (at 20°C) or 64 (at 25°C), respectively. Therefore, in case water seeps into the dry rock formation, a great variation of the dielectric property will take place.

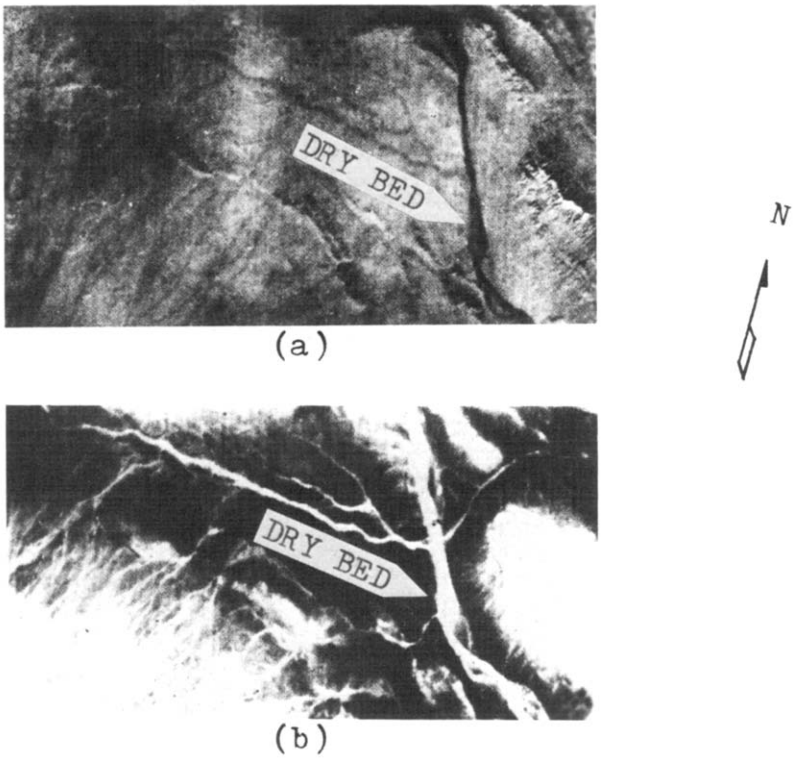

FIGURE 7. Infrared images of the longest dry bed which were acquired at noon (a) and night (b).

In spite of the extremely dry climate at Paergang, the moisture content of the faults zone, tectonic lines, and some dry beds appear to be slightly higher than that of surrounding rocks. That is an essential factor that brings about a "cold" microwave signature. The measurement shows that ϵ' of the sandy soil, one of the compositions making up the surface tectorium of the longest dry bed, is about 6 and is higher than the value (about 4) obtained under the perfectly dry condition. Unfortunately, we have not obtained sufficient *in situ* ground truth of moisture profiles to confirm this finding. The infrared scanning images (8–14 μm) have also proved that the moisture content of the longest dry bed is slightly higher than that of surrounding rocks. Figure 7 represents a central section of the longest dry bed [see Figure 3(b), C], where the water system appears in the darkest tone in Fig. 7(a) acquired at noon. Its infrared radiometric temperature has been found lower of the order of 2°C than that of surrounding rocks. On the contrary, the water system appears in the brightest tone in Figure 7(b) acquired at night. Its infrared radiometric temperature turns out to be higher of the order of 1°C than that of surrounding rocks. It has been found that it is the difference of the moisture content that causes the thermal inertia.

The laser altimeter synchronously recorded the relative height variations of topography at the same time as the microwave radiometric measurement was made. Based on viewing at nadir, with

horizontal polarization, the microwave radiometry theory suggests that the brightness temperature will decrease as surface slope increases (unless the surface is very rough at scales comparable to the wavelength). In fact, the average difference in height at the Paergang district is not great except for the Quege Mountain, where the average slope of the dry bed is about 1.4°. Undoubtedly, the effect of surface slope variations can be neglected for the longest dry bed and some taphrogeosyncline, at which the topography appears comparatively flat. As a result, the anomalous microwave signature there should be attributed to the moisture content effect. For the Quege Mountain, the effect of surface slope variations, however, has to be taken into consideration, although it might not be so serious as caused by the properties of rocks and minerals.

Conclusions

The qualitative analysis for the microwave radiometry data indicated conclusions as follows: First, the brightness temperature of rocks and minerals in the arid region is in the range of 230–280 K. The microwave signatures of various rocks and minerals depend mainly on their dielectric properties. Second, the fault zones and tectonic lines often give a lower brightness temperature, based on the substantial effect of water on microwave frequencies. It is reputed that the geologic structures associated with water and minerals, such as the faults, anticlines, and tectonic lines, likely act as reservoirs or oil traps and contain some mineral deposits originating from hydrothermal solutions. For indirect prospecting by searching for the geologic structures, it stands to reason that passive microwave radiometry can play a certain role. In this respect, it is necessary that research work in the laboratory is combined with field trials and that remote sensing techniques including microwave radiometry are combined with conventional geophysical exploration.

The authors wish to express their thanks to: Associate Scientist Zhang Junrong and all scientific and technological workers of the Microwave Remote Sensing Group, Changchun Institute of Physics, for their contributions in developing the microwave radiometer; Associate Scientist Tong Qingxi and Mr. Wang Changyao for their help in flight tests; Associate Scientist Zhu Wenman and Mr. Yan Fujun for their advice and assistance.

References

Bradford, W. R., and Plaster, M. (1973), Microwave radiometry and imaging, in *Handbook of Remote Sensing Techniques* (W. R. Bradford, Ed.), London, EMI Electronics Ltd., pp. 145–171.

Edgerton, A. T., and Trexler, D. T. (1970), A study of microwave techniques applied to geologic problems, U. S. Geological Survey Report No. 1361 R-1.

Hoekstra, P., and Cappilino, P. (1971), Dielectric properties of sea and sodium chloride ice at UHF and microwave frequencies, *J. Geophys. Res.* 76:4922–4931.

Vickers, R. S., and Rose, G. C. (1971), The use of complex dielectric constant as a diagnostic tool for the remote sensing of terrestrial materials, Colorado State University, Fort Collins, Colorado, Scientific Report No. 5.

Zhang Junrong (1980), Development of null-balancing microwave radiometer, in *Proceedings of the Symposium on Airborne Remote Sensing Tests at Hami District, Xinjiang* (Tong Qingxi, Ed.), Institute of Remote Sensing Application, Beijing, pp. 25–38 (in Chinese).

Received 14 July 1982; revised 15 April 1983.